nature photonics

ARTICLES

PUBLISHED ONLINE: 28 SEPTEMBER 2014 | DOI: 10.1038/NPHOTON.2014.219

Access to long-term optical memories using photon echoes retrieved from semiconductor spins

L. Langer[1], S. V. Poltavtsev[1,2], I. A. Yugova[2], M. Salewski[1], D. R. Yakovlev[1,3], G. Karczewski[4], T. Wojtowicz[4], I. A. Akimov[1,3]* and M. Bayer[1,3]

The ability to store optical information is important for both classical and quantum communication. Achieving this in a comprehensive manner (converting the optical field into material excitation, storing this excitation, and releasing it after a controllable time delay) is greatly complicated by the many, often conflicting, properties of the material. More specifically, optical resonances in semiconductor quantum structures with high oscillator strength are inevitably characterized by short excitation lifetimes (and, therefore, short optical memory). Here, we present a new experimental approach to stimulated photon echoes by transferring the information contained in the optical field into a spin system, where it is decoupled from the optical vacuum field and may persist much longer. We demonstrate this for an n-doped CdTe/(Cd,Mg)Te quantum well, the storage time of which could be increased by more than three orders of magnitude, from the picosecond range up to tens of nanoseconds.

Photon echoes are amazing optical phenomena, in which resonant excitation of a medium by short optical pulses results in a delayed response in the form of a coherent optical flash. Since their first observation in ruby in 1964[1], photon echoes have been reported for atom vapours[2], rare earth crystals[3] and semiconductors[4–6]. Spontaneous (two-pulse) and stimulated (three-pulse) photon echoes have been demonstrated and used for studying the energy levels and coherent evolution of optical excitations[7–9]. At present there is great interest in the application of photon echoes for quantum memories[10,11]. Photon echoes occur in an ensemble of oscillators with an inhomogeneous distribution of optical transitions. Such an ensemble provides high efficiency and large bandwidth, allowing the storage of multiple photons with high capacity. Current research efforts regarding photon echoes have mainly concentrated on rare earth crystals and atomic vapours with long storage times, which are crucial for the implementation of robust light–matter interfaces.

In the early stages of photon echo experiments, the spin level structure of ground and excited states was recognized to contribute to the formation of spontaneous and stimulated photon echo signals[12–14]. If optically addressed states have orbital and/or spin angular momenta, then the splitting of these states by a magnetic field (the Zeeman effect) provides an additional degree of freedom for the control of photon echoes through optical selection rules[15–17]. Moreover, coherent transfer from optical to spin excitations[18,19] has been suggested to considerably extend storage times, as demonstrated for quasi-atomic systems with comparable optical and spin coherence times[20]. However, coherent operations in quasi-atomic systems cannot be performed faster than on nanosecond or even longer timescales due to the low oscillator strength of the optical transitions. Here, we demonstrate for a semiconductor that the ultrashort picosecond optical pulses and the weak transverse magnetic field applied in our experimental protocol can lead to the transfer of a short-lived optical excitation into a long-lived electron spin state. This allows stimulated photon echoes to be induced with high bandwidth on submicrosecond timescales, exceeding the radiative lifetime of the optical excitations by more than three orders of magnitude. We reveal two mechanisms leading to this extension of stimulated echo revival—coherent transfer and spin fringes—and show that, depending on the polarization configuration of the three involved laser pulses, we are able to shuffle the optical field into a spin component that is directed either along or perpendicular to the magnetic field. The possibility of addressing all three spin components, and in particular also the one along the magnetic field, makes our approach highly appealing for future applications in memory devices.

Photon echoes from trions in zero magnetic field

To demonstrate magnetic-field-induced stimulated photon echoes we studied a semiconductor CdTe/(Cd,Mg)Te quantum well, a model system that can be tailored for targeted applications at a detailed level by means of nanotechnology. The fundamental optical excitations in semiconductors—excitons—have large oscillator strength, so resonant absorption may be achieved with close to unity efficiency, even for structure thicknesses smaller than the light wavelength. Accordingly, propagation effects are not as important as in atomic vapours and rare-earth crystals.

Ultrafast coherent spectroscopy of excitons employing laser pulses is well established for semiconductor nanostructures[8]. However, for storage applications, excitons have rarely been considered because of their limited optical coherence time T_2, due to their complex many-body interactions and their short radiative lifetime ($T_1 \leq 1$ ns) (a downside of the large oscillator strength). In nanostructures such as quantum dots, the optical decoherence is weak but still limited by radiative decay. Recently, therefore, approaches involving the long-lasting spin coherence of resident electrons have been pursued. Most such studies have focused on optical control of the spin, which implies spin manipulation and readout by optical fields[21–24]. The storage and retrieval of an optical field by encoding it in an ensemble of electron spins has not yet been addressed.

[1]Experimentelle Physik 2, Technische Universität Dortmund, 44221 Dortmund, Germany, [2]Spin Optics Laboratory, Saint Petersburg State University, 198504 St Petersburg, Russia, [3]A.F. Ioffe Physical-Technical Institute, Russian Academy of Sciences, 194021 St Petersburg, Russia, [4]Institute of Physics, Polish Academy of Sciences, PL-02668 Warsaw, Poland. *e-mail: ilja.akimov@tu-dortmund.de

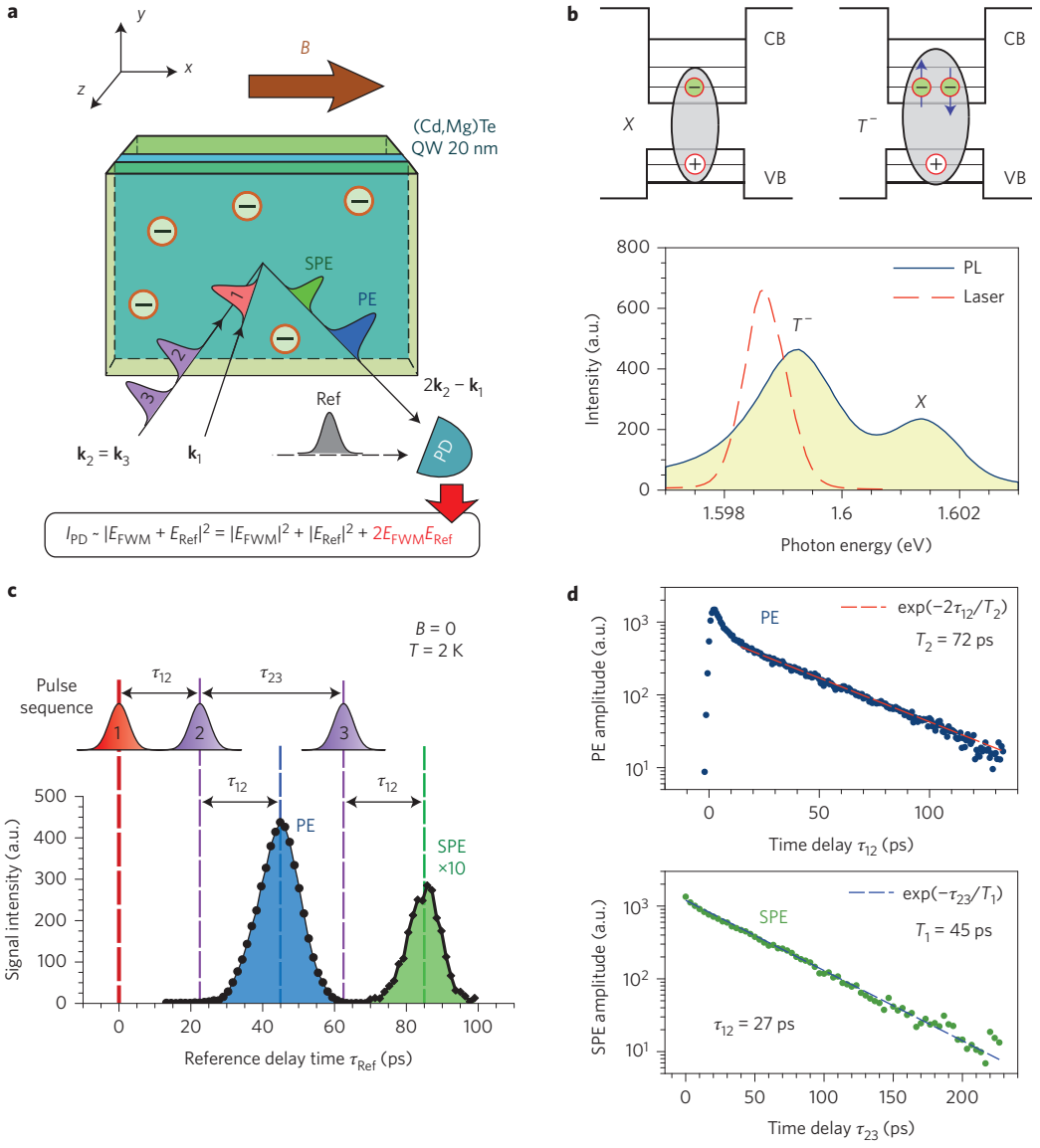

Figure 1 | Scheme of the photon-echo experiment and optical properties of the investigated structure. a, The CdTe/(Cd,Mg)Te quantum well (QW) is optically excited with a sequence of three laser pulses with variable delays τ_{12} and τ_{23} relative to each other. The resulting four-wave mixing (FWM) transients $|E_{FWM}(t)|$ are detected with the photodiode (PD) in the $2\mathbf{k}_2 - \mathbf{k}_1$ direction using a heterodyne technique. All measurements are performed at 2 K. **b**, Top: schematic presentation of exciton *X* and trion T^- complexes in the quantum well. The quantum well potential of conduction (CB) and valence (VB) bands leads to spatial trapping of electrons and holes. Bottom: photoluminescence spectrum (solid line) measured for above-barrier excitation with photon energy 2.33 eV, demonstrating *X* and T^- emission. The laser spectrum (dashed line) used in the photon-echo experiment is tuned to the low-energy flank of the T^- emission line. a.u., arbitrary units. **c**, FWM transients for $\tau_{12} = 23$ ps and $\tau_{23} = 39$ ps. PE and SPE signals appear at $\tau_{Ref} = 2\tau_{12}$ and $\tau_{Ref} = 2\tau_{12} + \tau_{23}$, respectively. **d**, Decay of PE and SPE peak amplitudes. From exponential fits (dashed lines) we evaluate $T_2 = 72$ ps and $T_1 = 45$ ps.

Figure 1 summarizes the experimental approach and the main results regarding the optical properties of the studied quantum well in zero magnetic field. We use a sequence of three excitation pulses with variable delays τ_{12} between pulses 1 and 2 and τ_{23} between pulses 2 and 3. The duration of the pulses $\tau_p \approx 2$–3 ps. Pulses 2 and 3 are propagating along the same direction, so their wavevectors are equal ($\mathbf{k}_2 = \mathbf{k}_3$). Both the spontaneous (PE) and stimulated (SPE) photon echoes are then directed along the $2\mathbf{k}_2 - \mathbf{k}_1$ direction. Transients are measured by taking the cross-correlation of the resulting four-wave mixing (FWM) signal $E_{FWM}(t)$ with the reference pulse $E_{Ref}(t)$ using heterodyne detection, as shown schematically in Fig. 1a (see Methods). This allows the PE and SPE signals to be distinguished because of their different arrival times at the detector.

Essential for the present experiment is the selection of a well-defined spin level system, optically excitable according to clean selection rules. Accordingly, we did not select the neutral exciton, but instead chose the charged exciton consisting of two electrons and a hole, which requires a resident electron population. The studied sample was composed of 20-nm-thick CdTe quantum wells separated by 110 nm $Cd_{0.78}Mg_{0.22}Te$ barriers. The barriers were doped with donors, which provide resident electrons for the quantum wells, with density $n_e \approx 1 \times 10^{10}$ cm^{-2}. At the experimental cryogenic temperature of 2 K, these electrons become localized in quantum well potential fluctuations due to the well width and variations in composition[25]. In the photoluminescence spectrum, both the neutral (*X*) and charged exciton (in short, trion T^-) are observed, separated by the trion binding energy. In the T^- ground

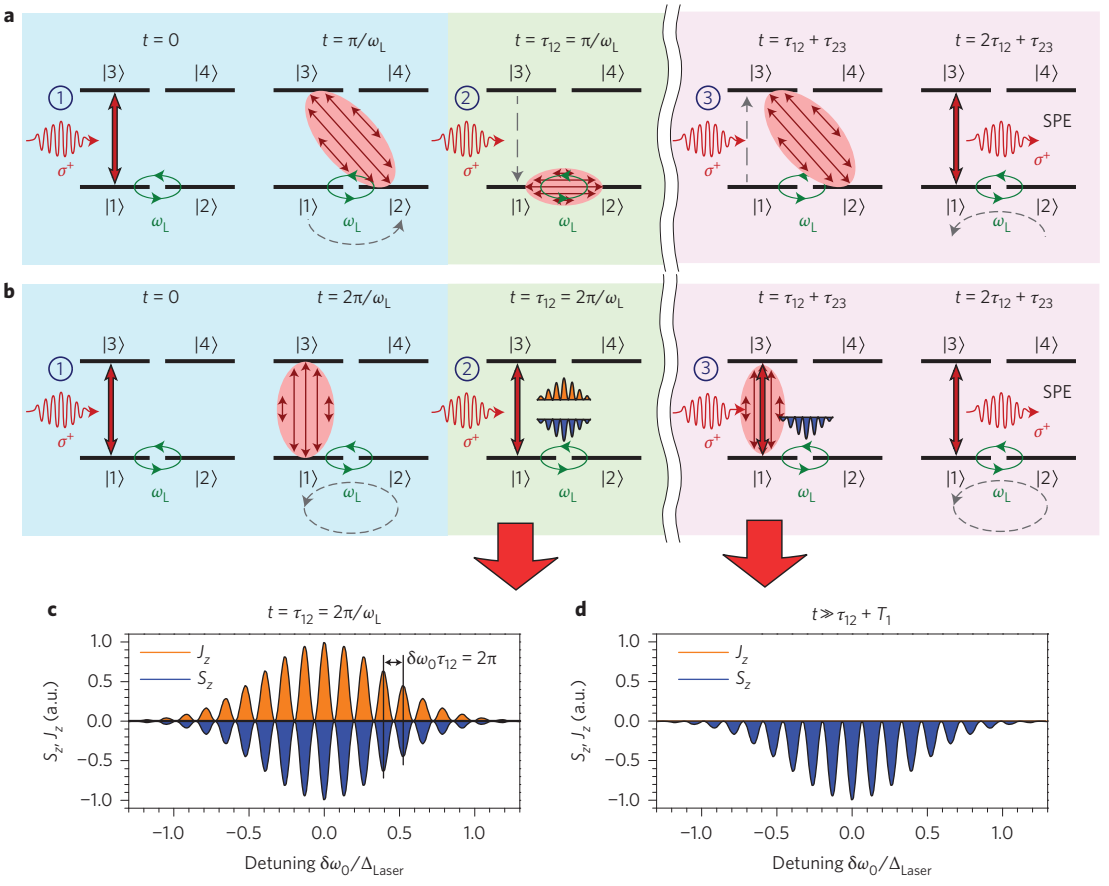

Figure 2 | Schematic presentation of the main mechanisms responsible for magnetic-field-induced SPE. The main three stages of optical initialization, storage and readout are highlighted in blue, green and violet, respectively. Optical pulses are circularly polarized. **a**, Coherent transfer of optical excitation into electron spin (S_x and S_y components). The efficiency is maximum for $\tau_{12} = \pi/\omega_L$. **b**, Creation of spectral spin fringes for electrons and trions (S_z and J_z components). This mechanism is most efficient for $\tau_{12} = 2\pi/\omega_L$. **c**,**d**, The spectral spin gratings for electrons and trions are shown at the moment of creation by the second pulse ($t = \tau_{12} = 2\pi/\omega_L$) (**c**) and after trion recombination and before the arrival of pulse 3 ($t \gg \tau_{12} + T_1$) (**d**). a.u., arbitrary units.

state, the two electrons form a spin singlet state. The narrow widths of the spectral lines indicate a high structural quality (Fig. 1b). It is worth mentioning that localization of an electron at a donor located in the quantum well is also possible. In this case the optical transitions between donor bound electron and donor bound exciton (D^0X) are addressed. Most importantly, however, the same SPE scenarios are valid for the trion and donor-bound exciton complexes.

To address solely the optical transition from electron to trion, the photon energy of the laser was tuned to the lower energy flank of the trion emission line, namely $\hbar\omega = 1.599$ eV. In this way we also selectively excited T^- complexes with enhanced localization, which have longer optical coherence times. The laser spectrum is shown by the dashed line in Fig. 1b. Figure 1c gives the characteristic FWM signal taken at $\tau_{12} = 23$ ps and $\tau_{23} = 39$ ps, while the delay τ_{Ref} of the reference pulse is scanned relative to pulse 1. Signatures of PE and SPE are clearly seen in the transients: the PE signal appears at $\tau_{Ref} = 2\tau_{12}$ and the SPE at $\tau_{Ref} = 2\tau_{12} + \tau_{23}$ (ref. 7). The decay of the PE and SPE peak amplitudes with increasing τ_{12} and τ_{23}, respectively, is shown in Fig. 1d. From these data we evaluate decay times of $T_2 = 72$ ps and $T_1 = 45$ ps so that $T_2 \approx 2T_1$, indicating that the loss of coherence for the trions is mainly due to radiative decay with lifetime $\tau_r = T_1$.

The investigated electron–trion transition can be considered as a four-level system, as shown schematically in Fig. 2. Note that the density of electrons in the quantum well is low (exciton Bohr radius $a_B \ll \sqrt{n_e}$), which allows us to consider the resident electrons as isolated, non-interacting carriers. Many-body interactions are weak for localized carriers and can be neglected at the low excitation densities used in our experiment[26]. We resonantly excited optical transitions between the doubly degenerate electron states with spin projections $S_z = \pm 1/2$ (ground states $|1\rangle$ and $|2\rangle$) and the doubly degenerate trion states with spin projections $J_z = \pm 3/2$ (excited states $|3\rangle$ and $|4\rangle$). The excited-state spin projections are determined by the heavy-hole total angular momentum because the trion electrons form a singlet state ($S = 0$). The selection rules for optical excitation follow from angular momentum conservation, that is, $|1\rangle + \sigma^+ \rightarrow |3\rangle$ and $|2\rangle + \sigma^- \rightarrow |4\rangle$. Here, σ^+ and σ^- denote the corresponding circular photon polarizations. At zero magnetic field the transitions are decoupled. In addition, the spin relaxation time of holes (T_h) and electrons (T_e) are long compared to the radiative lifetime (T_e, $T_h \gg \tau_r$)[25]. The SPE signal is therefore expected to decay with $T_1 = \tau_r$ when the delay τ_{23} is increased, in full accord with the experimental data in Fig. 1d. In the next section we explain the main mechanisms that emerge in the magnetic field using the scheme in Fig. 2. Although we describe the interaction of matter with $\pi/2$ light pulses for clarity, all conclusions are valid for low-power excitation (see Supplementary Sections 1.2 and 1.5), as manifested by our experimental data.

Coherent transfer and spin fringes

Application of an external magnetic field in the quantum well plane, $\mathbf{B} \parallel \mathbf{x}$, leads to Larmor precession of the electron spin in the ground state. In this way, the transfer of an optical excitation into a long-lived electron spin state can be achieved, and a dramatic increase

in the SPE decay time by several orders of magnitude may be accomplished. The whole process comprises three steps: (1) pulse 1 creates the optical excitation (initialization—conversion of the optical field into a material excitation), (2) pulse 2 performs a transformation of the optical excitation into the spin system (storage), and (3) pulse 3 induces the SPE (readout). There are two different mechanisms contributing to the magnetic-field-induced signal (Fig. 2). The first (Fig. 2a) is based on direct transfer of a coherent superposition from optical excitation into the electron spin system and the second (Fig. 2b) is based on desynchronization of the spectral fringes for electron and trion spins.

For simplicity, let us consider a situation where the pulse duration τ_p is significantly shorter than the period of Larmor precession $T_L = 2\pi/\omega_L = 2\pi\hbar/g\mu_B B$, where g is the electron g-factor and μ_B is the Bohr magneton. Under these conditions the selection rules for optical transitions remain unchanged. For both mechanisms (Fig. 2a,b) it is important that the Larmor precession frequencies of the trion and electron spins are different. This is perfectly the case in quantum well structures where confinement along the z-direction splits the heavy-hole and light-hole bands and therefore the optically excited trion states do not become coupled by the weak transverse magnetic field because of the in-plane heavy-hole g-factor, $g_{hh} \approx 0$ (ref. 27). This feature simplifies the analysis of the system's time evolution because one only has to account for Larmor precession of the electron spin, that is, a periodic exchange between S_y and S_z with frequency ω_L. For simplicity, we also consider the following relations between the time constants, which realistically represent the situation for the studied electron–trion system and correspond also to the most interesting case of long-lived echoes:

$$T_L \leq \tau_{12} \ll T_2 \tag{1}$$

$$T_1 \ll \tau_{23} \ll T_e \quad \text{and} \quad T_1 \ll T_h \tag{2}$$

The first relation requires fast Larmor spin precession and conservation of coherence for optical excitation before the arrival of pulse 2. The second relation limits our consideration to arrival times of pulse 3 after trion recombination; that is, the system is in the ground state at $t = \tau_{23}$ and all required information is stored in the electron spin. Here, we recall that $\tau_r \approx T_1 \approx T_2/2$. If relations (1) and (2) hold, the solutions of the Lindblad equation of motion for the (4×4) density matrix ρ_{ij}, which describes the four-level electron–trion system, can be written in a compact form. For the electron spin components containing the required terms with $\exp(-i\omega_0\tau_{12})$ time evolution (see Supplementary Equation (22)) we obtain

$$S_x = \frac{\rho_{12} + \rho_{21}^*}{2} \propto K\Sigma \sin\left(\frac{\omega_L\tau_{12}}{2}\right)\exp\left(-\frac{\tau_{23}}{T_1^e}\right) \tag{3}$$

$$S_y = \frac{\rho_{12} - \rho_{21}^*}{2i} \propto K\Delta \sin\left(\frac{\omega_L\tau_{12}}{2} + \omega_L\tau_{23}\right)\exp\left(-\frac{\tau_{23}}{T_2^e}\right) \tag{4}$$

$$S_z = \frac{\rho_{11} - \rho_{22}}{2} \propto -K\Delta \cos\left(\frac{\omega_L\tau_{12}}{2} + \omega_L\tau_{23}\right)\exp\left(-\frac{\tau_{23}}{T_2^e}\right) \tag{5}$$

Here $K = \exp[-i(\omega_0\tau_{12} - \mathbf{k}_1\mathbf{r} + \mathbf{k}_2\mathbf{r})]\exp(-\tau_{12}/T_2) + c.c.$ is the term that carries the information on the optical phase, $\Delta = \theta_{1+}\theta_{2+} - \theta_{1-}\theta_{2-}$ and $\Sigma = \theta_{1+}\theta_{2+} + \theta_{1-}\theta_{2-}$ account for $\sigma^{\pm}$ light polarization of the excitation pulse n with pulse area $\theta_{n\pm} \ll 1$. T_1^e and T_2^e correspond to the longitudinal and transverse electron spin relaxation times, respectively, and ω_0 is the trion resonance frequency. Here, we assume that, initially, before the arrival of pulse 1 ($t < 0$), the electron spins are unpolarized, that is, $\rho_{11} = \rho_{22} = 1/2$, while all other elements of the density matrix vanish. From equations (3) to (5) it follows that at $B > 0$ all spin components are finite with magnitudes depending critically on the polarization of the exciting pulses. Note that a sequence of two pulses (pulses 1 and 2) performs spin initialization of the resident electrons in a way that is very similar to a spin-flip stimulated Raman process[28–30].

Qualitatively, the magnetic-field-induced SPE evolution is easy to follow for a circularly polarized pulse sequence, as shown in Fig. 2. At $t = 0$, pulse 1 creates a coherent superposition between states $|1\rangle$ and $|3\rangle$. This is an optical coherence associated with the ρ_{13} element of the density matrix. Due to inhomogeneous broadening of optical transitions, this coherence ρ_{13} disappears due to dephasing. Each dipole in the ensemble with a particular optical frequency ω_0 acquires an additional phase $\varphi(t) = (\omega - \omega_0)t = \delta\omega_0 t$ before the arrival of the second pulse at $t = \tau_{12}$ (see term K in equations (3) to (5)). This is indicated by a set of arrows with different lengths, symbolizing the phase distribution of the dipoles with different frequencies.

The first mechanism (Fig. 2a) is most efficient when the second pulse arrives at $\tau_{12} = (2m + 1)\pi/\omega_L$, where m is an integer; that is, optical coherence ρ_{13} is shuffled into a ρ_{23} coherence between the optically inaccessible pair of states $|2\rangle$ and $|3\rangle$. Pulse 2 transfers this coherence into a superposition of states $|1\rangle$ and $|2\rangle$, corresponding to spin coherence $\rho_{12} = S_x - iS_y$ (see equations (3) and (4)). There, the coherence is frozen in the ground state without any further optical dephasing and can survive for much longer times than the zero-field coherence, even after the radiative trion recombination time τ_r. Note, however, that the Larmor precession of the electron spin continues then. Dephasing of the S_y component may therefore occur, while S_x decays on a longer timescale with T_1^e as it is directed along the magnetic field (see equations (3) and (4)). Finally, pulse 3 retrieves the coherence ρ_{12} by converting it back into the optical frequency domain and starting the rephasing process. Here, the rephasing will be most efficient if $\rho_{12}(t = \tau_{12} + \tau_{23}) = \rho_{12}^*(t = \tau_{12})$, that is, for $\tau_{23} = (2l + 1)\pi/\omega_L$, where l is an integer. We emphasize that this mechanism is different from the standard stimulated photon echo where the second pulse projects the quantum state onto a given axis (population grating), leading consequently to a partial loss of information. Here, a complete transformation of a coherent superposition between optically coupled states into the electron spin is established, which is essential for quantum optical applications.

The second mechanism (Fig. 2b) can be considered to be an incoherent one. In contrast to the first, it relies on population rather than coherence. Here, the accumulated phase of each dipole φ is projected by pulse 2 into population interference fringes $\rho_{11} \propto \sin^2(\delta\omega_0\tau_{12}/2)$ and $\rho_{33} \propto \cos^2(\delta\omega_0\tau_{12}/2)$, that is, into spectral population gratings in the excited and ground states with opposite phase[7]. These are equivalent to spectral spin fringes for the electrons ($S_z = (\rho_{11} - \rho_{22})/2$) and trions ($J_z = (\rho_{33} - \rho_{44})/2$). In contrast to the previous mechanism, the interference fringes have the highest contrast when the second pulse arrives after an integer number of electron spin revolutions $t = \tau_{12} = 2m\pi/\omega_L$ (equation (5)). For $t > \tau_{12}$ the Larmor precession of the electron spin desynchronizes the spin fringes in ground and excited states. Therefore, even after trion recombination, the electron spin grating does not disappear. Spin fringes $S_z(\delta\omega_0)$ and $J_z(\delta\omega_0)$ are schematically shown in Fig. 2c,d for two different times: the time of their creation $t = \tau_{12}$ and the time after trion recombination before the arrival of pulse 3. Accordingly, a long-lived electron spin grating is present, allowing one to retrieve the phase information φ and observe the SPE pulse with maximum signal at $\tau_{23} = l\pi/\omega_L$.

Photon echo from electron spin system

In practice, the initial condition of zero electron spin polarization is hard to match for circularly polarized pulse sequences. This is because σ^+ excitation induces a macroscopic spin polarization.

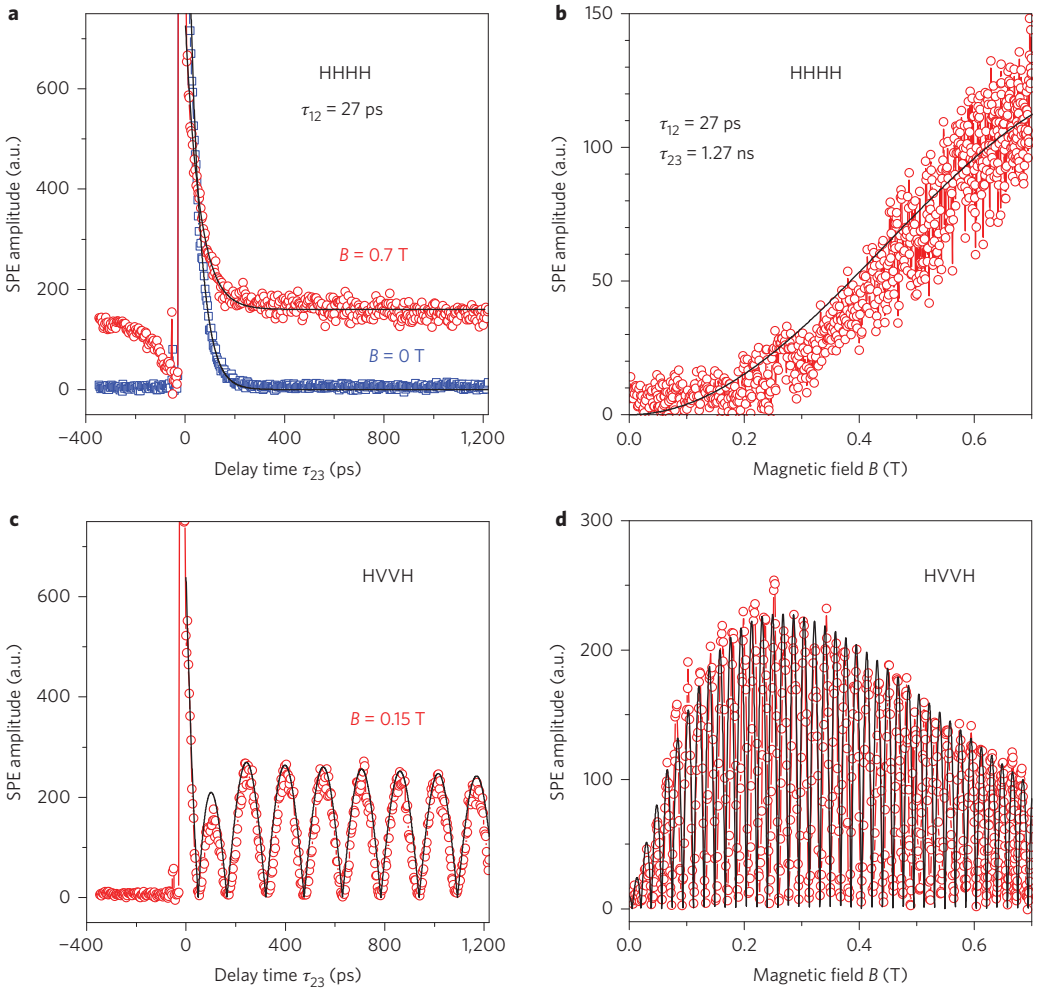

Figure 3 | Experimental demonstration of magnetic-field-induced long-lived SPE. The delay time τ_{12} is set to 27 ps. **a**, Stimulated echo amplitude, in arbitrary units (a.u.), in configuration HHHH as a function of time delay τ_{23} at $B = 0$ and 0.7 T. **b**, Long-lived part of the stimulated echo amplitude as a function of magnetic field. Symbols are experimental data. Black curves in **a** and **b** present theoretical calculations with parameters $|g| = 1.52$, $\tau_r = 43$ ps, $T_h = 1{,}000$ ps and $T_1^e \approx 50$ ns. **c**, Stimulated echo amplitude in configuration HVVH as a function of delay τ_{23} at $B = 0.15$ T. **d**, Long-lived part of stimulated echo amplitude versus magnetic field. Black curves in **c** and **d** are calculations with parameters $|g| = 1.52$, $\Delta g = 0.018$, $\tau_r = 43$ ps, $T_h = 1{,}000$ ps and $T_2^e > T_R$.

The electron spin relaxation $T_2^e \approx 30$ ns is longer than the pulse repetition period $T_R = 13.2$ ns in our experiment and $\mathbf{S}(t = 0) \neq 0$ (ref. 25). Moreover, for arbitrary τ_{12}, both mechanisms are present and therefore all spin components contribute to the SPE signal. Circularly polarized pulses are therefore not optimal for the demonstration of magnetic-field-induced SPE. From equations (3) to (5) it follows that a linearly polarized pulse sequence is much more attractive. For linearly $H = (\sigma^+ + \sigma^-)/\sqrt{2}$ or $V = (\sigma^+ - \sigma^-)/\sqrt{2}$ co-polarized pulses, $\Delta = 0$ and $\Sigma = 2\theta_1\theta_2$, so only the dephasing-free S_x component is involved. Here, we exploit only the first mechanism (Fig. 2a) of coherent transfer. If pulses 1 and 2 are cross-polarized, the opposite situation, with $\Delta = 2\theta_1\theta_2$ and $\Sigma = 0$, is obtained. Here, the S_y and S_z components contribute. The corresponding SPE amplitudes are given by

$$P_{\mathrm{HHHH}} \propto \sin^2\left(\frac{\omega_L \tau_{12}}{2}\right)\exp\left(-\frac{\tau_{23}}{T_1^e}\right) \quad (6)$$

$$P_{\mathrm{HVVH}} \propto \cos\left[\omega_L(\tau_{12}+\tau_{23})\right]\exp\left(-\frac{\tau_{23}}{T_2^e}\right) \quad (7)$$

where the polarization sequence is denoted by the subscript ABCD, with A, B and C corresponding to the polarizations of pulses 1, 2 and 3, respectively, and D being the polarization of the resulting SPE pulse (see Supplementary Section 1.5). Note that the SPE echo in the HVVH configuration oscillates with the Larmor precession frequency in dependence on $\tau_{12} + \tau_{23}$, while in the HHHH configuration it varies only with the τ_{12} delay time. The decay of the signals is also different. For HVVH the decay occurs according to the transverse spin relaxation time T_2^e, and additional dephasing due to the electron g-factor inhomogeneity Δg may play a role. In HHHH the signal decays with the longitudinal spin relaxation time T_1^e.

The experimental data for the SPE amplitude as a function of delay time τ_{23} and magnetic field B, measured in the HHHH and HVVH polarization configurations, are summarized in Fig. 3. The delay time between pulses 1 and 2 is set to $\tau_{12} = 27$ ps, which corresponds to $\tau_{12}/T_L = 0.40$ at $B = 0.7$ T and $\tau_{12}/T_L = 0.086$ at $B = 0.15$ T. For comparison, the SPE decay measured at $B = 0$ is shown in Fig. 3a. The magnetic field dependence of the SPE amplitude in Fig. 3b,d is measured for $\tau_{23} = 1.27$ ns, which is significantly longer than the radiative lifetime T_1. Note that the experimentally measured signal corresponds to the absolute value of amplitude $|P|$. In full accord with our expectations, we observe a long-lived SPE signal when applying the magnetic field. The theoretical curves are in good agreement with the data. The calculations take into account the full

dynamics of the system, including the excited states, and therefore also reproduce the short decay component of the SPE due to trion recombination as well as the signals at low magnetic fields with $T_L > \tau_{12}$ (see Supplementary Equations (26) and (28)).

In the case of HHHH, no oscillations appear when τ_{23} is varied (Fig. 3a), which is in line with equation (6). Particularly fascinating is the observation of SPE signal at negative delays ($\tau_{23} \approx -300$ ps) at a 75% level of the SPE amplitude at positive delays ($\tau_{23} \approx 300$ ps) (Fig. 3a). This means that within the pulse repetition period of 13 ns the SPE amplitude reduces by only 25%. From these data we estimate $T_1^e \approx 50$ ns, which allows us to observe SPE signals in the magnetic field on a submicrosecond timescale. The short dynamics at negative delays (-200 ps $< \tau_{23} < 0$) is due to the excitation of trions by pulse 3, which influences the initial conditions at $t = 0$. Note that for the linearly polarized pulse sequence no macroscopic spin polarization becomes involved in the PE experiment due to inhomogeneous broadening of the optical transitions. We therefore obtain information about the intrinsic longitudinal spin relaxation of the electron spin. The experimental data demonstrate that classical storage of light in S_x is feasible and attractive, because this spin component, being parallel to **B**, is robust against relaxation and is not sensitive to dephasing.

The oscillatory signal in the HVVH polarization configuration corresponds to the electron g-factor $|g| = 1.52$. It decays on a timescale of several nanoseconds due to dephasing of the electron spin ensemble, which is determined by the g-factor inhomogeneity. No SPE signal is therefore observed at negative delays (Fig. 3c). The reduction of the SPE signal for $B > 0.3$ T in Fig. 3d is also related to this fact. From fitting the data we evaluate $\Delta g = 0.018$. The use of dynamic decoupling protocols based on spin echoes with microwave radiation should allow one to extend the signal significantly to tens of nanoseconds[31].

In conclusion, we have demonstrated magnetic-field-induced long-lived stimulated photon echoes in the electron–trion system. By appropriate choice of the polarization pulse sequence the optical field can be transferred into spin directed along or perpendicular to a magnetic field. Although no metastable states are involved due to the long-lived electron spin coherence, the timescale of echo stimulation can be extended by more than three orders of magnitude over the optical coherence time in the quantum well system. Note that the electron–trion energy level structure is identical in quantum wells and self-assembled quantum dots. We used quantum wells for demonstration, because the trion transitions are well isolated spectrally. As a down side, we had to keep the excitation power low in order to suppress many-body effects. In the case of singly charged quantum dot structures, $\pi/2$ and π pulses can be efficiently used for coherent manipulation[32]. In addition, the longitudinal spin relaxation times in, for example, (In,Ga)As quantum dots may be as long as 0.1 s (ref. 33). Further exploiting the hyperfine interaction between electrons and nuclei might enable storage times of seconds or longer[34]. Therefore, our findings open a new avenue for the realization of optical memories in semiconductor nanostructures.

Methods

The semiconductor quantum well structure was grown by molecular-beam epitaxy, and was composed of five electronically decoupled 20-nm-thick CdTe quantum wells embedded in 110 nm $Cd_{0.78}Mg_{0.22}Te$ barriers[25]. The barriers were doped by iodine donors, which provide the quantum well layers with CB electrons of low density $n_e \approx 1 \times 10^{10}$ cm^{-2}. The sample was mounted in a liquid-helium bath cryostat at a temperature of 2 K. Magnetic fields up to 0.7 T were applied in a Voigt geometry using an electromagnet. The direction of the magnetic field was parallel to the quantum well plane (**B** || **x**).

We used a tunable self-mode-locked Ti:sapphire laser as the source of optical pulses with durations of 2–3 ps at a repetition rate of 75.75 MHz (repetition period $T_R = 13.2$ ns). The laser was split into four beams. Three were used for the three-pulse sequence required to stimulate the photon echo, and the fourth was used as a reference pulse in the heterodyne detection. The delay between all four pulses could be scanned by reflectors mounted on mechanical translation stages. The three-pulse FWM experiment was performed in reflection geometry. Pulse 1 with wavevector $\mathbf{k}_1$ impacted the sample at an incidence angle of ~6°. Pulses 2 and 3 both travelled along the same direction ($\mathbf{k}_2 = \mathbf{k}_3$), which was different from that of the first beam, and impacted the quantum well structure at an incidence angle of ~7°. The beams were focused onto the sample at a spot with a diameter of ~200 μm. The intensities of each pulse were selected to remain in the linear excitation regime; that is, the FWM intensity depended linearly on the intensity of each of the beams (pulse energy of ~10–100 nJ cm^{-2}). The FWM signal was collected along the $2\mathbf{k}_2 - \mathbf{k}_1$ direction. We used interferometric heterodyne detection, where the FWM signal and reference beam are overlapped at a balanced detector[35]. The optical frequencies of pulse 1 and the reference pulse were shifted by 40 MHz and 41 MHz with acousto-optical modulators. The resulting interference signal at the photodiode was filtered by a high-frequency lock-in amplifier selecting $|2\omega_2 - \omega_1 - \omega_{Ref}| = 1$ MHz. This provided a high-sensitivity measurement of the absolute value of the FWM electric field amplitude in real time when scanning the reference pulse delay time τ_{Ref}, which was taken relative to the pulse 1 arrival time. The polarization of the excitation pulses, as well as the detection polarization, were controlled with retardation plates in conjunction with polarizers.

Received 19 January 2014; accepted 20 August 2014; published online 28 September 2014

References

1. Kurnit, N. A., Abella, I. D. & Hartmann, S. R. Observation of a photon echo. *Phys. Rev. Lett.* **13,** 567–568 (1964).
2. Mossberg, T., Flusberg, A., Kachru, R. & Hartmann, S. R. Total scattering cross section for Na on He measured by stimulated photon echoes. *Phys. Rev. Lett.* **42,** 1665–1669 (1979).
3. Takeuchi, N. & Szabo, A. Observation of photon echoes using a nitrogen laser pumped dye laser. *Phys. Lett. A* **50,** 361–362 (1974).
4. Schultheis, L., Sturge, M. & Hegarty, J. Photon echoes from two-dimensional excitons in GaAs–AlGaAs quantum wells. *Appl. Phys. Lett.* **47,** 995–997 (1985).
5. Noll, G., Siegner, U., Schevel, S. G. & Göbel, E. O. Picosecond stimulated photon echo due to intrinsic excitations in semiconductor mixed crystals. *Phys. Rev. Lett.* **64,** 792–795 (1990).
6. Webb, M. D., Cundiff, S. T. & Steel, D. G. Observation of time-resolved picosecond stimulated photon echoes and free polarization decay in GaAs/AlGaAs multiple quantum wells. *Phys. Rev. Lett.* **66,** 934–937 (1991).
7. Wiersma, D. A. & Duppen, K. Picosecond holographic-grating spectroscopy. *Science* **237,** 1147–1154 (1987).
8. Chemla, D. S. & Shah, J. Many-body and correlation effects in semiconductors. *Nature* **411,** 549–557 (2001).
9. Samartsev, V. V. Coherent optical spectroscopy of promising materials for solid-state optical processors. *Laser Phys.* **20,** 383–446 (2010).
10. Lvovsky, A. I., Sanders, B. C. & Tittel, W. Optical quantum memory. *Nature Photon.* **3,** 706–714 (2009).
11. Hammerer, K., Sørensen A. S. & Polzik, E. S. Quantum interface between light and atomic ensembles. *Rev. Mod. Phys.* **82,** 1041–1093 (2010).
12. Lambert, L. Q., Compaan, A. & Abella, I. D. Modulation and fast decay of photon-echos in ruby. *Phys. Lett. A* **30,** 153–154 (1969).
13. Chen, Y. C., Chiang, K. & Hartmann, S. R. Photon echo relaxation in LaF_3:Pr^{3+} *Opt. Commun.* **29,** 181–185 (1979).
14. Morsink, J. B. S., Hesselink, W. H. & Wiersma, D. A. Photon echo stimulated from optically induced nuclear spin polarization. *Chem. Phys. Lett.* **64,** 1–4 (1979).
15. Alekseev, A. I., Basharov, A. M. & Beloborodov, V. N. Photon-echo quantum beats in a magnetic field. *J. Phys. B* **16,** 4697–4715 (1983).
16. Rubtsova, N. N. *et al.* Non-Faraday rotation of photon-echo polarization in ytterbium vapor. *Phys. Rev. A* **70,** 023403 (2004).
17. Langer, L. *et al.* Magnetic-field control of photon echo from the electron-trion system in a CdTe quantum well: shuffling coherence between optically accessible and inaccessible states. *Phys. Rev. Lett.* **109,** 157403 (2012).
18. Scully, M. O. & Zubairy, M. S. in *Quantum Optics* Ch. 7 (Cambridge Univ. Press, 1997).
19. Berman, P. R. & Malinovsky, V. S. in *Principles of Laser Spectroscopy and Quantum Optics* Ch. 9 (Princeton Univ. Press, 2011).
20. Afzelius, M. *et al.* Demonstration of atomic frequency comb memory for light with spin-wave storage. *Phys. Rev. Lett.* **104,** 040503 (2010).
21. Greilich, A. *et al.* Mode locking of electron spin coherences in singly charged quantum dots. *Science* **313,** 341–345 (2006).
22. Press, D., Ladd, T. D., Zhang B. & Yamamoto, Y. Complete quantum control of a single quantum dot spin using ultrafast optical pulses. *Nature* **456,** 218–221 (2008).
23. Berezovsky, J., Mikkelsen, M. H., Stoltz, N. G., Coldren, L. A. & Awschalom, D. D. Picosecond coherent optical manipulation of a single electron spin in a quantum dot. *Science* **320,** 349–352 (2008).
24. Xu, X. *et al.* Coherent population trapping of an electron spin in a single negatively charged quantum dot. *Nature Phys.* **4,** 692–695 (2008).

25. Zhukov, E. A. *et al.* Spin coherence of a two-dimensional electron gas induced by resonant excitation of trions and excitons in CdTe/(Cd,Mg)Te quantum wells. *Phys. Rev. B* **76,** 205310 (2007).
26. Zhukov E. A. *et al.* Optical control of electron spin coherence in CdTe/(Cd,Mg) Te quantum wells. *Phys. Rev. B* **81,** 235320 (2010).
27. Debus, J. *et al.* Spin-flip Raman scattering of the neutral and charged excitons confined in a CdTe/(Cd,Mg)Te quantum well. *Phys. Rev. B* **87,** 205316 (2013).
28. Hu, P., Geschwind, S. & Jedju, T. M. Spin-flip Raman echo in n-type CdS. *Phys. Rev. Lett.* **37,** 1357–1360 (1976).
29. Carter, S. G., Chen, Z. & Cundiff S. T. Ultrafast below-resonance Raman rotation of electron spins in GaAs quantum wells. *Phys. Rev. B* **76,** 201308 (2007).
30. Press, D. *et al.* Ultrafast optical spin echo in a single quantum dot. *Nature Photon.* **4,** 367–370 (2010).
31. Lovrić, M., Suter, D., Ferrier, A. & Goldner, P. Faithful solid state optical memory with dynamically decoupled spin wave storage. *Phys. Rev. Lett.* **111,** 020503 (2013).
32. Zrenner, A. *et al.* Coherent properties of a two-level system based on a quantum-dot photodiode. *Nature* **418,** 612–614 (2002).
33. Kroutvar, M. *et al.* Optically programmable electron spin memory using semiconductor quantum dots. *Nature* **432,** 81–84 (2004).
34. Oulton, R. *et al.* Subsecond spin relaxation times in quantum dots at zero applied magnetic field due to a strong electron–nuclear interaction. *Phys. Rev. Lett.* **98,** 107401 (2007).
35. Langbein W. & Borri P. in *Semiconductor Qubits* (eds Henneberger, F. & Benson, O.) Ch. 12, 269 (Pan Stanford, 2008).

Acknowledgements

The authors thank V.S. Zapasskiĭ for discussions. The Dortmund team acknowledge financial support from the Deutsche Forschungsgemeinschaft, the Bundesministeriuum für Bildung und Forschung (project Q.com-H). The project 'SPANGL4Q' acknowledges financial support from the Future and Emerging Technologies (FET) programme within the Seventh Framework Programme for Research of the European Commission, under FET-Open grant no. FP7-284743. S.V.P. thanks the Russian Foundation of Basic Research for partial financial support (contract no. 14-02-31735 mol-a). S.V.P. and I.A.Yu. acknowledge partial financial support from the Russian Ministry of Science and Education (contract no. 11.G34.31.0067), SPbU (grants nos. 11.38.67.2012 and 11.38.213.2014) and the Skolkovo Institute of Science and Technology (in the framework of the SkolTech/MIT Initiative). I.A.A. and M.B. acknowledge partial financial support from the Russian Ministry of Science and Education (contract no. 14.Z50.31.0021). The research in Poland was partially supported by the National Science Center (Poland) under grants nos. DEC-2012/06/A/ST3/00247 and DEC-2014/ST3/266881.

Author contributions

L.L., S.V.P., M.S. and I.A.A. performed the experiments and analysed the data. I.A.Y. developed the theoretical model. G.K. and T.W. fabricated the samples. I.A.A., M.B., D.R.Y., S.V.P. and I.A.Y. conceived the idea for the experiment and co-wrote the paper. All authors discussed the results and commented on the manuscript.

Additional information

Supplementary information is available in the online version of the paper. Reprints and permissions information is available online at www.nature.com/reprints. Correspondence and requests for materials should be addressed to I.A.A.

Competing financial interests

The authors declare no competing financial interests.